Modeling Photonic Links in Verilog-A

by

Ekaterina Kononov

B.S. E.E., MIT (2012)

Submitted to the Department of Electrical Engineering and Computer Science
in partial fulfillment of the requirements for the degree of

Master of Engineering in Computer Science and Engineering

at the

MASSACHUSETTS INSTITUTE OF TECHNOLOGY

June 2013

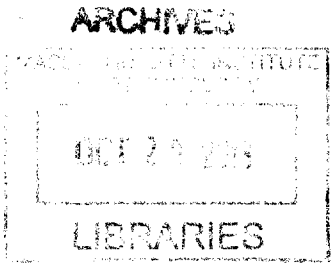

Author .....
Department of Electrical Engineering and Computer Science
May 24, 2013

Certified by .....
Vladimir Stojanovic
Associate Professor
Thesis Supervisor

Accepted by .....
Prof. Dennis M. Freeman
Chairman, Masters of Engineering Thesis Committee

Modeling Photonic Links in Verilog-A

by

Ekaterina Kononov

Submitted to the Department of Electrical Engineering and Computer Science
on May 24, 2013, in partial fulfillment of the
requirements for the degree of
Master of Engineering in Computer Science and Engineering

Abstract

Integrated photonic links are a promising emerging technology that can relieve the interconnect bottleneck in core-to-core and core-to-memory communications of modern processors. Developing and optimizing photonic link systems requires simulation of integrated photonic devices side-by-side with electronic devices at the device, circuit, and system level. In previous efforts to simulate photonic links, the optical and the electrical signals were treated in separate simulators, which resulted in some loss of accuracy. In this thesis, a library of photonic device models is developed in Verilog-A for use in seamless simulation of opto-electronic circuits in Cadence.

Thesis Supervisor: Vladimir Stojanovic
Title: Associate Professor

Acknowledgments

Everyone in ISG, especially everyone on the photonics project. In particular, Mike who taught me the basics and sparked my interest in the beginning, Jonathan who made invaluable contibutions to the project with his Verilog expertise. Special thanks to Cheri for her patience in each of the many times she explained to me how a ring modulator works. Most importantly, Vladimir under whose supervision I stayed on-task and on-schedule.

Contents

List of Figures

List of Tables

Chapter 1

Introduction

As Moore's Law scaling of transistors starts to reach a quantum limit, processor manufacturers have turned to parallelism with many-core systems. However, even parallel processing is beginning to offer diminishing returns due to the increasing strain of communication networks. Interconnections between the cores and on-chip L2 caches, as well as off-chip DRAM, consume a significant portion of the die area and power budget. Limitations of I/O pin pitch on the package and power density constraints reduce the link bandwidth. Key performance metrics of a communication link are bandwidth, latency, and energy cost per bit. Traditional interconnect technology is reaching a point where it is impossible to improve in one metric without making sacrifices in the others.

A novel technology, silicon photonics, is a promising solution to the communication bottleneck. The integrated photonic link offers high bandwidth density using dense wavelength division multiplexing (DWDM). Photonic links can provide 10Tb/s/mm^2 bandwidth density at a 8Gb/s data rate, a significant advantage over electrical links [1]. The projected improvement in bandwidth density over electrical links is 32-64x for on-chip links and 130-260x for off-chip links [3].

Unlike traditional interconnect, photonic links do not suffer from sensitivity to electromagnetic interference or low pass filtering characteristics, offering better signal integrity. Furthermore, the energy cost per bit is independent of distance because no energy is spent charging and discharging parasitic wiring capacitance, which also

means that no off-chip drivers or buffers are needed. Because DWDM circumvents the I/O pin limitation, the link can run at slower, more energy efficient data rates. Photonic links offer many advantages over traditional electrical links.

1.1 The Need for Models

Before the developing photonic link technology can become a mainstream part of integrated circuits, its various trade-offs must be explored. This thesis aims to model a photonic link in a way that is compatible for simulation alongside electrical devices, circuits, and systems. Side-by-side simulation of the optical and electrical domains will allow us to accurately capture the costs and trade-offs of photonic technology.

The rest of the thesis is organized as follows. Chapter 2 overviews photonic technology and the modeling language, Verilog-A. Chapter 3 summarizes previous efforts on modeling photonic links. Chapter 4 presents our work on modeling photonic links. Chapter 5 showcases our models' functionality by presenting simulation results.

Chapter 2

Background

In this chapter we present the background information needed to understand this project. First we overview the operation of a photonic link and present the components comprising the link which will be modeled. Next is an explanation of Verilog-A, the language used for modeling the components.

2.1 Photonic Link Overview

Photonic links can be used for both intra-chip and chip-to-chip communications. One of the most salient features of photonic links is wavelength division multiplexing (WDM), which allows bidirectional communication of multiple senders and receivers using the same physical waveguide. The following section illustrates the use of WDM.

2.1.1 An Example Photonic Link

Figure 2-1 shows an example intra-chip link which takes advantage of WDM. In this example, an external laser source generates two carrier waves, one with wavelength λ_1 and the other with wavelength λ_2. The two waves are coupled into the plane of the chip using a vertical grating coupler. Next, the waves approach the ring modulator for *Sender A*. Since *Sender A*'s ring has its resonance tuned to λ_1, that wave couples into the ring and *Sender A* modulates a stream of data onto it with

on-off keying. Meanwhile, λ_2 passes the ring unaffected. Next, the waves approach the ring modulator for *Sender B*, which is tuned to λ_2. *Sender B* modulates data onto λ_2 while λ_1 passes unaffected. At the other end of the link, the ring filter for *Receiver A* is tuned to pick off λ_1 and route it into a photodetector. The ring filter for *Receiver B* does the same for λ_2. A this point, a receiver circuit translates each of the received light intensities into digital bits in the electrical domain.

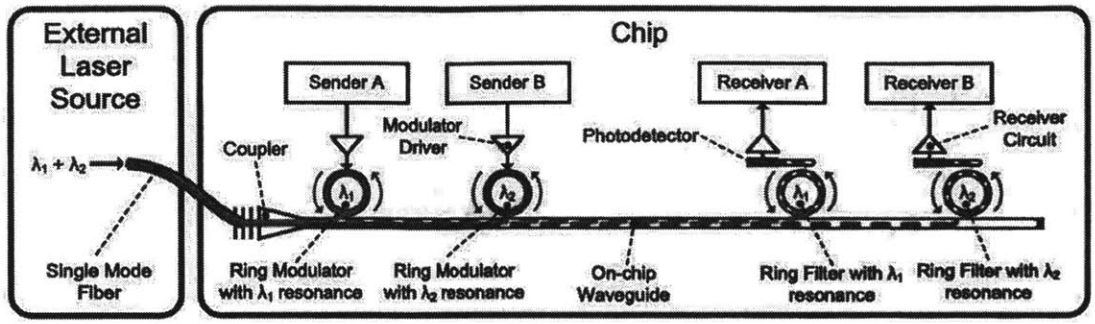

Figure 2-1: An intra-chip photonic link illustrating wavelength division multiplexing. *Sender A* communicates with *Receiver A* and *Sender B* communicates with *Receiver B* using the same waveguide but different wavelengths λ_1 and λ_2.

Furthermore, chip-to-chip links such as the one shown in Figure 2-2 take advatage of the insensitivity of the energy cost per bit to the distance that bit needs to be sent. The link in Figure 2-2 also illustrates the bidirectionablity achievable with WDM. In this link, *Chip A* uses λ_1 to send data to *Chip B*, and *Chip B* uses λ_2 to send data to *Chip A* using the same modulator and receiver ring filter components at the intra-chip link in Figure 2-1. Moreover, like that intra-chip link, this chip-to-chip link can also have two or more sets of senders and recievers by introducing λ_3 and λ_4 and so on, but still sharing the same waveguide.

2.1.2 Photonic Link Components

As evident in the previous section, photonic links consist of several components. The sections below will describe each component in the order that they appear in the example link.

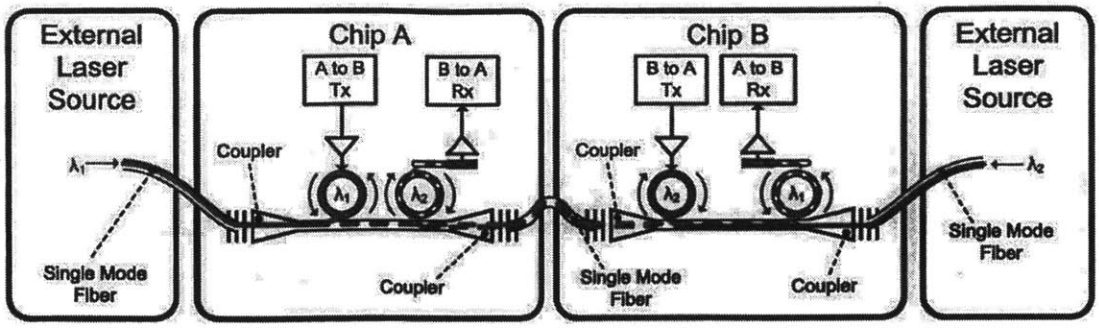

Figure 2-2: A chip-to-chip photonic link illustrating bidirectionality. *Chip A* sends data to *Chip B* using λ_1 and *Chip B* sends data to *Chip A* using λ_2 using the same waveguide.

Laser Source

The laser source can be integrated on-chip or an external off-chip source. Monolithic inegration constrains us to build all devices out of silicon, but due to the indirect bandgap of silicon there is no high-efficiency laser source known [2]. Therefore, we use a continuous-wave external laser source with wavelengths in the 1200nm-1500nm range.

Vertical Grating Coupler

A vertical grating coupler allows light to be directed into and out of the plane of the chip. At the surface of the die, the coupler is dimensioned at about 10x10μm, and a bragg-grating structure tapers into the waveguide of width 0.5μm [2]. We use vertical grating couplers to couple the external last source through a fiber optic wire into the photonic structures under test.

Waveguide

Waveguides are used to route light to various points within a chip. They are fabricated in the poly-silicon layer, which is the same layer as the gate of the transistor. A waveguide is composed of a silicon core, with high index of refraction, which is surrounded by a cladding material of a lower index. To reduce optical mode leakage losses, a post-processing procedure etches away silicon substrate under the waveguide

to form an air gap, as shown in Figure 2-3 [2]. The air gap increases the index contrast between the waveguide core and its cladding, allowing waveguide bend radii of a just few microns with low loss [1].

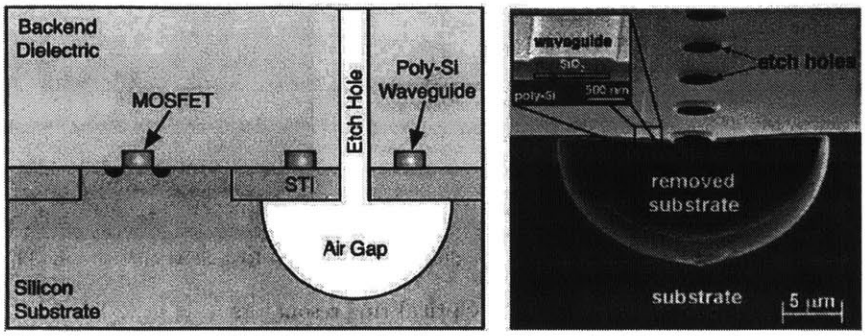

Figure 2-3: Diagram and SEM Micrograph of waveguide fabricated in bulk CMOS using undercut air gap to reduce loss.

Ring Resonator

A ring resonator is a loop of waveguide with radius typically less than 10μm. It is used for wavelength-selective filtering. When the circumference of the ring is equal to an integer number of wavelengths, there is resonance and the light becomes trapped in the ring so that the ring acts as a notch filter for that wavelength. The resonant wavelength can be changed with device geometry, thermal tuning using a resistive heater, or changing the index of refraction, which is applied in the modulator.

Modulator

The modulator encodes data onto the light stream. A modulator, diagramed in Figure 2-4, consists of a ring filter where portions of the ring are lined with N-type and P-type polysilicon to form PIN diodes. Due to limitations in fabricating curved structures on a Manhattan grid, the ring is stretched into a racetrack shape so that the PIN diodes can be constructed on the straight sections.

Light is modulated by shifting the stop band of the ring filter in and out of the optical channel using the diodes. Forward biasing the diodes causes carrier injection and reverse biasing causes carrier depletion, each one of which changes the index of

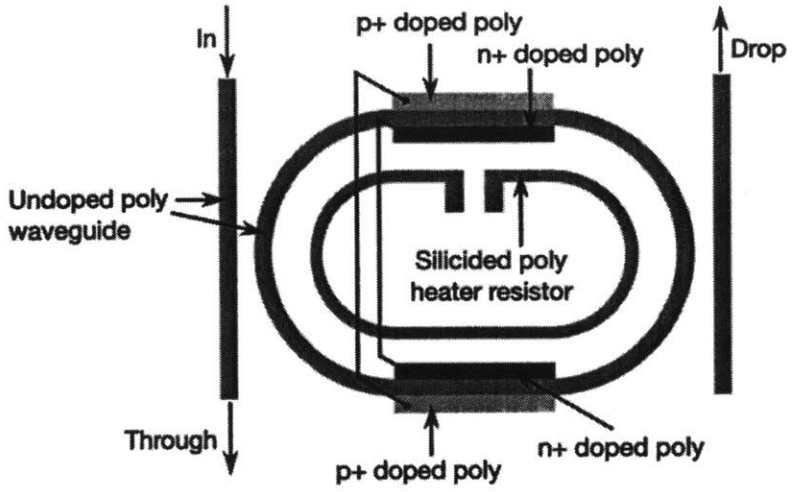

Figure 2-4: Diagram of ring modulator.

refraction of the ring. This index change causes phase shift in the light, and thereby changes the resonant frequency of the ring.

The optical response of the modulator is the time that the resonance takes to build up, and it depends on the quality factor (Q) of the resonant ring. The higher the Q the slower the response. On the other hand, the electrical response of the modulator can be slow for carrier-injection modulators with long carrier lifetimes, so techniques like pre-emphasis [3] had to be developed to speed up the electrical response. Carrier-depletion modulators seem to offer a faster electrical response. Since carrier-injection modulators have high power consumption and self-heating effects due to carrier recombination in the forward biased junction, we chose to work on the more efficient reverse-biased carrier-depletion modulator.

Photodetector

A photodetector contains a photodiode which converts optical power into electrical current. When light is absorbed in the intrinsic region of the PIN diode, an electron and hole pair is generated. The charge carriers are swept away by the electric field across the junction, generating a current. The small current is sensed and resolved into a digital 1 or 0 by a receiver circuit such as in [4].

Photodiodes are made with a silicon-germanium alloy, where the fraction of germanium determines the wavelength range which can be absorbed [2]. Therefore, a photodiode on its own is wideband - it needs a ring filter to drop a single frequency on it. In the example link in Figure 2-1, there is a ring filter which routes light of the correct wavelength to each photodetector, but Figure 2-5 shows a different photodetector in which the PIN diodes are built into the ring. This technique reduces the area used for the photodetector and decreases laser power required for bit resolution by leveraging the resonant nature of the ring.

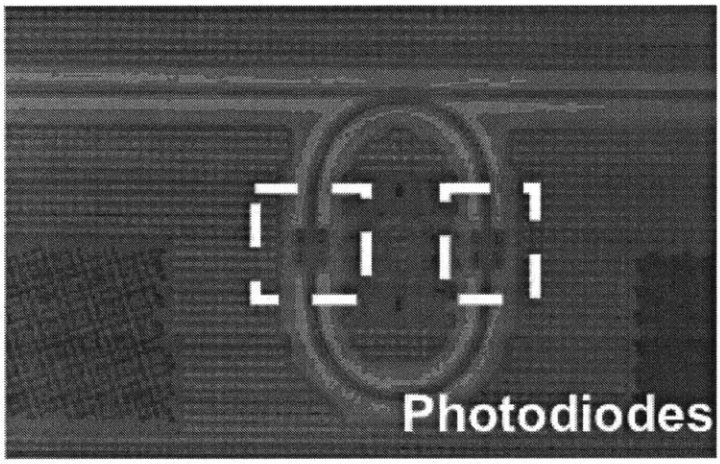

Figure 2-5: Die photograph of photodetector with photodiodes indicated [12].

2.2 Verilog-A

Verilog-A is a hardware description language (HDL) which supports multi-disciplinary components, such as mechanical, thermal, fluidic, and in our case optical. In addition, Verilog-A leverages abstraction which allows representation of components as behavioral models rather than as transistor-level circuits, which can greatly shorten simulation time.

The flexibility in modeling multi-disciplinary components comes from Verilog-A's construct of a discipline. A discpline is a collection of related physical signal types which are called natures [5]. For example, in the electrical discipline, two natures are

voltage and current. Disciplines and natures are defined in a separate file which is included in each model. For this project, we defined an optical discipline which has an electric field nature.

In Verilog-A relationships between signals on ports are defined with contribution statements. For example, there can be multiple contribution statements for the current between two ports, some depeding on the voltage. The simulation engine solves the system of equations so that the total current is the sum of all contributions.

This work describes a library of models for photonic components written in Verilog-A. Verilog-A is appealing for modeling photonic links because the models are compatible for use in the circuit design flow alongside electrical components, and therefore will allow the design and optimization of truly integrated opto-electronic systems. In previous works, the optical components of a system had to be simulated in a separate simulator from the electrical components, which is not as accurate because the results didn't reflect the effects they had on each other. Nevertheless, previous work on modeling provided a foundation for this thesis, so it is summarized in the following chapter.

Chapter 3

Previous Work

While this thesis presents the first set of photonic models written in Verilog-A, previous work on modeling photonic components has been done at Carleton University. These researchers colaborated with Optiwave Systems to create a simulator called OptiSPICE [6]. They suggested the key idea of representing light inside a photonic device as magnitude and phase of an electric field, and they described their methodolgy for modeling several devices for simulation in OptiSPICE [7] [8] [9]. Although this thesis describes models written in Verilog-A for simulation in Cadence, the work done at Carleton provided an essential starting point for this project.

3.1 OptiSPICE, a Photonics Simulator

OptiSPICE is a time-domain spice-compatible simulator which simulates optical circuits using a technique called Modified Nodal Analysis (MNA). First, preprocessing algorithms compute mode shapes and effects of interfaces to characterize devices for equation creation. Then system equations are created in the form

$$\mathbf{C}\frac{d\mathbf{x}}{dt} + \mathbf{G}\mathbf{x} + \mathbf{F}(\mathbf{x}) = \mathbf{B}(t)$$

where $\mathbf{C}$ represents energy storage, $\mathbf{G}$ is the conductance matrix, $\mathbf{F}$ is a set of nonlinear functions describing the elements, $\mathbf{B}$ is the forcing function, and $\mathbf{x}$ is the vector

of state variables [7]. The simulator uses Newton-Raphson iterations to find the DC starting point and numerical integration to find solutions for each time step. It keeps track of four variables at each node: magnitude and phase of the forward and backward propagating wave, as shown in Figure 3-1. Using magnitude and phase as state variables allows efficient use of nonuniform time stepping which outweighs computation time spent treating interference devices as nonlinear.

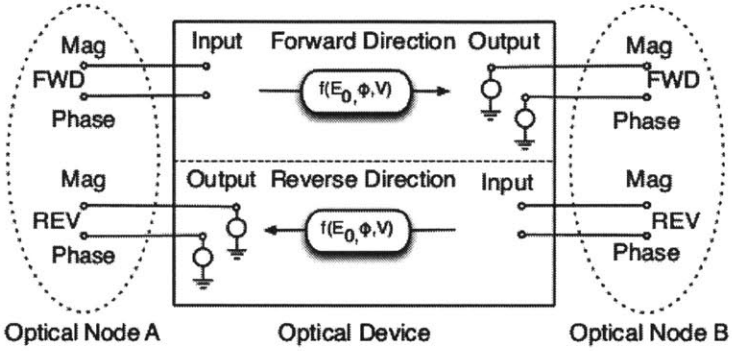

Figure 3-1: Block diagram of a generic optical device showing the four state variables computed at each node.

3.2 Magnitude and Phase

In order to simulate light traveling through a photonic link, the electric field needs to be calculated for various points of the link in various points in time. When light propagates through a waveguide, the total electric field at a particular point in the waveguide is described by the equation:

$$\bar{E}(t, z_0) = E_F(t)e^{j\phi_F(t)}e^{-j\omega_0 t} + E_B(t)e^{j\phi_B(t)}e^{j\omega_0 t}$$

where $E_i(t)$ is the time varying envelope and $\phi_i(t)$ is the time varying phase of the forward- or backward-propagating electromagnetic wave. The term $e^{j\omega_0 t}$ represents the THz carrier frequency of light. Keeping track of the THz oscillations of the electric field would force the simulator to use extremely small time steps, which is impractical. To avoid small time steps, the dependence on carrier frequency is removed, and the

equation becomes:

$$\bar{E}(t, z_0) = E_F(t)e^{j\phi_F(t)} + E_B(t)e^{j\phi_B(t)}$$

However, in order to take advantage of WDM, some notion of carrier frequency offset needs to be retained. Therefore, if the above equation represents the electric field of one channel with carrier frequency ω_0, then a second channel with carrier frequency $\omega_1 = \omega_0 + \Delta\omega$ can be represented as:

$$\bar{E}(t, z_0) = E_F(t)e^{j\phi_F(t)}e^{-j\Delta\omega t} + E_B(t)e^{j\phi_B(t)}e^{j\Delta\omega t}$$

Since all channels need to fit within one FSR of a ring resonator, the frequency offset $\Delta\omega$ will not be larger than several tens of GHz. Therefore, since $\Delta\omega \ll \omega_0$, the problem of extremely small time stepping is avoided.

3.3 Optical Devices

The optical devices modeled at Carleton University were categorized into three types: 1) direct elements, in which the signals remain in the optical domain; 2) sources and detectors, which convert electrical signals into optical signals or vice versa; and 3) interference elements, which linearly mix optical signals, but they are treated as nonlinear because trigonometry is used to compute their real and imaginary parts: $E_{real} = E_{mag}\cos\phi$, and $E_{imag} = E_{mag}\sin\phi$.

The main example of a direct element is multi mode waveguide which carries n channels with m bidirectional modes each. However, only a finite set of modes is excited with a significant amount of energy. Mode excitation is a function of device geometry and carrier wavelength [7]. Each additional mode included in the simulation adds two rows (forward and backward propagating) to the systeme equation matrices.

More direct devices include a unidirectional optoisolator, mirrors. Sources and detectors include the diode laser, continuous-wave source, and photodiode. Interference devices include optical connectors, combiners, cross couplers, ring filters. An optical connector, or optical scattering element (OSE), is a special non-physical de-

vice that was modeled for simulating scattering, transmission, and reflection effects at interfaces of actual devices [8].

Chapter 4

Models

This chapter describes how the Verilog-A model of a full photonic link was developed. First, a laser source was modeled, followed by the creation of a waveguide element. A version zero photodetector was made to allow output verification, and it was later refined to have photodiode characteristics. The modulator was also developed in steps: first a passive ring resonator device was created from a coupler and waveguide, and then the diode characteristic, which allows modulation, was added. The following sections will describe the underlying principles of each component model in detail.

4.1 Continuous-Wave Laser Source

The first model that we develop is the continuous-wave laser source because it allows us to provide an input signal for testing all subsequent components. A symbol of the laser source illustrating the electrical inputs and two-wire optical output port of the model is shown in Figure 4-1.

The model has an input port for laser output power and another port for frequency offset. We also provide an input port for temperature because the output of the laser is thermally dependent. Although we currently use an external laser source in the experimental setup, the model is made to support thermal characteristics of integrated laser sources as well. The relationship between the input signals and the

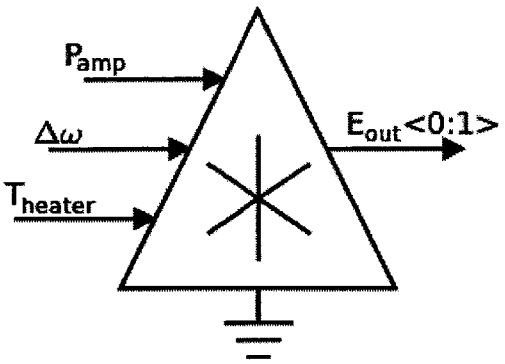

Figure 4-1: Symbol for laser model.

complex output is:

$$E_{out} = P_{amp} e^{j\,g \int_0^t \Delta\omega + T_{heater}(\tau)\,d\tau}$$

However, because Verilog-A does not support complex numbers, this translates into two signals:

$$\begin{aligned} E_{out}<0> &= E_{mag} = P_{amp} \\ E_{out}<1> &= E_{phase} = g \int_0^t \Delta\omega + T_{heater}(\tau)\,d\tau \end{aligned}$$

In this equation, $\Delta\omega$ is a constant offset frequency which is a parameter that can be set for each instance of the laser. The gain factor g is used to turn voltage into frequency because the frequency offset is input using a voltage source, but needs to be converted to frequency(1V increments laser frequency by $g/2\pi$ Hz). P_{amp} is laser output power in Watts, and T_{heater} is the temperature offset, which is currently used for thermal control of laser frequency. The output of the laser, E_{out}, is a two-wire bus in the optical domain, where one wire has the magnitude and the second wire has the phase of the output laser light.

4.1.1 PolToCart and CartToPol

At this point if the laser frequency had an offset from the nominal center frequency then the phase would grow linearly with time. It cannot be allowed to grow to infinity, so it had to be taken modulo $2\pi/\Delta\omega$. This caused the phase to be a sawtooth triangle

wave with an abrupt jump at every period of $2\pi/\Delta\omega$. To the simulator, this was a very large slope causing convergence problems and aphysical spikes to occur when simulating elements that involve derivatives.

To combat this problem, we made two blocks to convert the state variables magnitude and phase into real and imaginary parts that oscillate with a period of $2\pi/\Delta\omega$ but do not contain discontinuities. The blocks, called *PolToCart* and *CartToPol* are shown in Figure 4-2. These blocks were instatiated inside component models every time a conversion from cartesian to polar or vice versa was needed.

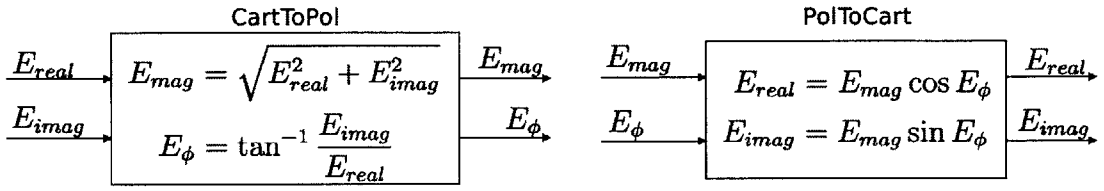

Figure 4-2: Cartesian-to-polar and Polar-to-cartesian converters.

4.2 Waveguide

The model of the waveguide needs to account for three effects that are experienced by light propagating through the waveguide: time delay, phase delay, and magnitude attenuation. The model can be broken down into blocks, one for each effect, as shown in Figure 4-3.

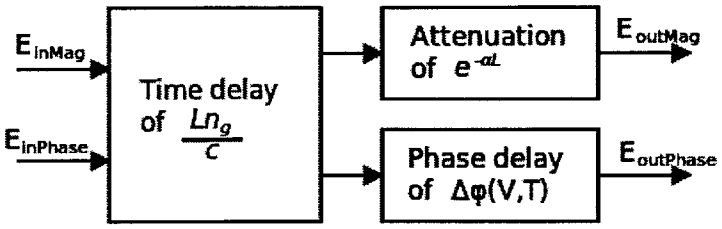

Figure 4-3: Waveguide modeled as three blocks.

Overall, the relationship between the incoming and outgoing light for the waveguide is described by

$$E_{out}(t) = |E_{in}(t - \frac{Ln_g}{c})|e^{-\alpha L}e^{j\omega\phi(t-\frac{Ln_g}{c})}$$

The field loss in the waveguide is determined by the attenuation term, $e^{-\alpha L}$. It is a function of the attenuation coefficient α and the waveguide length L, parameters that can be set for each instance. The time delay is the amount of time it takes for the light to traverse the length of the waveguide: $\frac{Ln_g}{c}$. The phase delay is left as 0 for the simple waveguide, but it becomes a function of voltage and temperature in the phase shifter portion of the modulator, discussed in Section 4.4.1.

4.3 Passive Ring Resonator

The ring resonator, or ring filter, is broken down into two blocks to simplify the device model, as shown in Figure 4-4. One block is simply an instance of a waveguide. Since the waveguide is circular in this case, the length parameter would be set based on the desired radius of the ring: $L = 2\pi r$. The following section describes how the second block, the cross-coupler, was implemented.

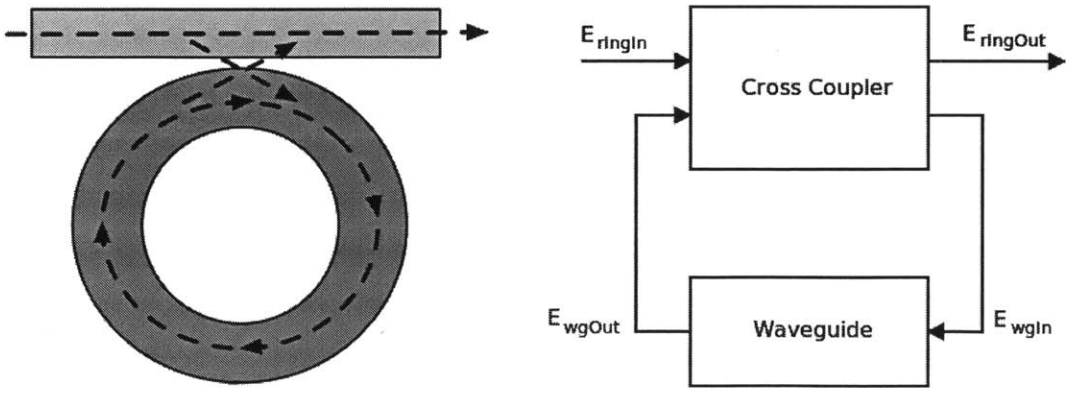

Figure 4-4: On the left is a ring resonator and on the right is a representation of it as a cross-coupler with a waveguide feedback path.

4.3.1 Cross-Coupler

The cross-coupler is a device which has two optical inputs and two optical outputs. The outputs are a mixture of the inputs:

$$\begin{bmatrix} E_{wgOut} \\ E_{ringOut} \end{bmatrix} = \begin{bmatrix} -it & \sqrt{1-t^2} \\ \sqrt{1-t^2} & -it \end{bmatrix} \begin{bmatrix} E_{ringIn} \\ E_{wgIn} \end{bmatrix}$$

In that equation, t is the field coupling coefficient which determines the proportions of each input mixed into the output. One input/output pair of the cross-coupler is the incoming and outgoing light of the ring filter. The second input/output pair is the incoming and outgoing light of the waveguide which comprises the circular portion of the ring.

4.3.2 Thermal Tuning of Ring Resonators

We model the temperature dependence of the ring resonator because temperature affects the index of refraction and hence the phase delay in the ring waveguide. We can take advantage of this effect to thermally tune the ring to a particular resonant frequency. Ring tuning corrects for the process variations that occur during fabrication: the resonance of a ring can shift away from the intended value by as much as 90GHz ring-to-ring on the same die and 600GHz die-to-die [1]. In addition, the die experiences time-dependent thermal fluctuations during operation (for example heating of the die due to power dissipation), which can shift the resonance of a ring in a CMOS process by -10GHz/K.

There are several ring tuning methods such as fully thermal, full athermalization using post-process trimming, windowed tuning to nearest resonance taking advantage of cyclical FSR, and electrically-assited tuning which uses carrier-depletion to further shift ring resonance [1]. Each method has different implications on the efficiency of the system as a whole, and therefore it is important to include thermal depencence and a temperature input port in the ring model. This is currently a work-in-progress, but the thermal dependence would be modeled by modifying the waveguide model,

replacing the group index n_g with a thermally dependent index $n(T)$.

4.4 Ring Modulator

The ring modulator encodes data onto the light stream by shifting the ring resonance in and out of the optical channel. The modulator has optical ports for the incoming and outgoing light. The electrical ports are the p and n ports of the diode that allows electrically shifting the resonance. The frequency response of the modulator is shown in Figure 4-5.

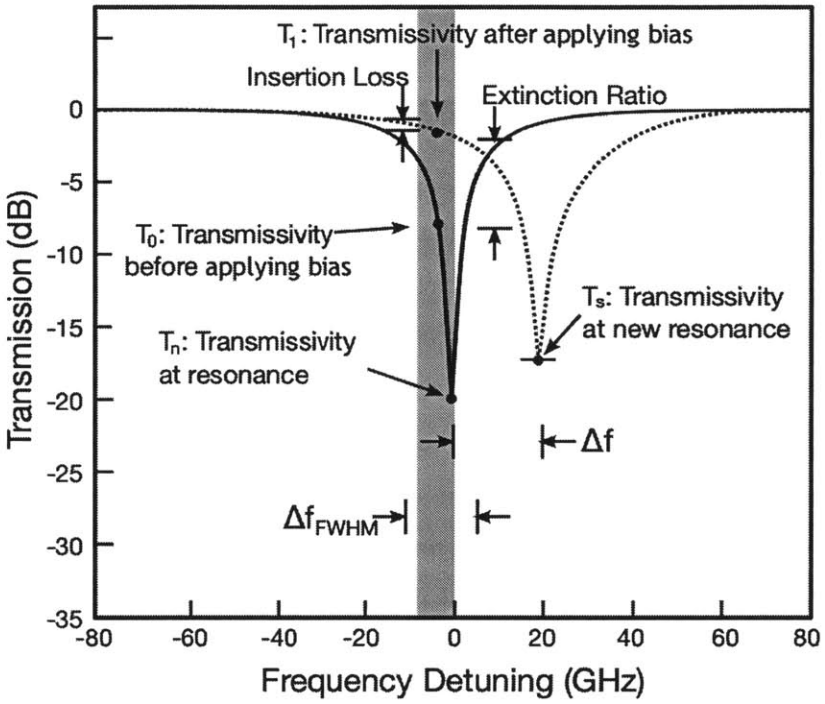

Figure 4-5: Shift in frequency response of a ring modulator due to application of voltage across the built-in diode.

The figure indicates two key parameters of a modulator: insertion loss and extinction ratio. Insertion loss (IL) is the ratio of input to output light intensity when modulator is outputting an optical 1. Extinction ratio (ER) is the ratio of light intensity between an optical 1 and an optical 0. Thus, an extinction ratio of 3dB is a twofold change in optical power between a 1 and a 0. When designing a modulator, it

is possible to calculate the charge needed to deplete from the pn-junction to achieve the desired ER and IL, and then to calculate the diode bias voltage needed to deplete that much charge.

In our model of the modulator, we do not compute a static transfer function. Instead, we split the device into two components, the same way that we did for the passive ring filter. One component is a cross-coupler. The other component, a phase shifter, is described in detail in the following section.

4.4.1 Phase Shifter

A modulator contains a ring resonator, so its model has much in common with the ring resonator model. However, the modulator is an active device because portions of the waveguide which makes up the ring are lined with diodes. Reverse biasing these diodes changes the index of refraction, shifting the phase of the light. To model this effect, the waveguide portion of the ring resonator is replaced with a configurable phase shifter element to make a modulator, shown in Figure 4-6. The relationship

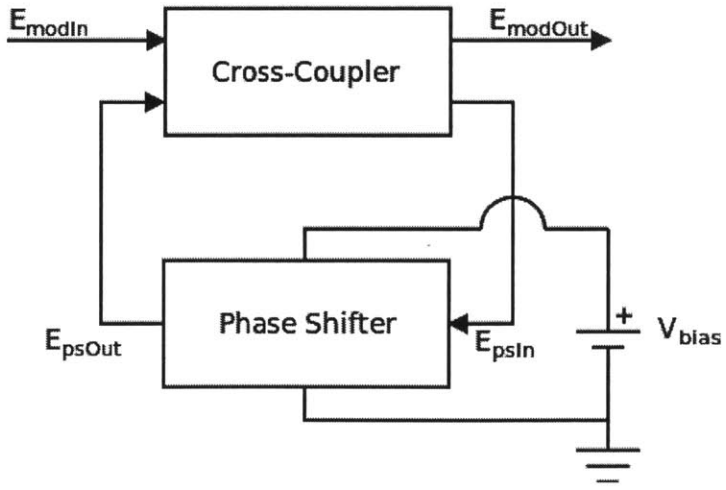

Figure 4-6: A ring modulator represented as a cross-coupler with a voltage-dependent phase shifter feedback path.

between the input and output light of the phase shifter is described by a similar equation to the waveguide, but the phase delay is now dependent on voltage applied

across the diode:

$$\begin{aligned} E_{out}(t) &= |E_{in}(t - \frac{Ln_{eff}}{c})|e^{-\alpha L}e^{j\omega\phi(t-\frac{Ln_{eff}}{c})} \\ n_{eff} &= n_0 + n_1 V_{bias} \end{aligned}$$

In this equation, n_{eff} is the new, effective index, which is a function of modulator bias voltage. The coefficients n_0 and n_1 are fitting numbers for the index response to applied voltage V_{bias}. In a more exact iteration of the model, n_{eff} will also be a function of temperature.

Since the phase shifter contains a diode, the relationship between current and voltage on the diode port is attributed diode characteristics:

$$\begin{aligned} I_{cap} &= \frac{d}{dt}(C(V_{bias})\, V_{bias}) \\ I_{res} &= I_s(e^{\frac{V_{bias}}{v_t}} - 1) \end{aligned}$$

The first equation accounts for the capacitance $C(V_{bias})$ of the p-n junction. This capacitance is a function of bias voltage, and for the first version of the model, the function is a polynomial fit to data collected from a Sentaurus simulation of a typical modulator device used on our test chips. The second equation is the Shockley diode equation, where the reverse-bias saturation current, I_s, is a parameter that can be set for each instance.

4.5 Photodetector

The photodetector contains a PIN diode that senses incoming light. The light impinging on the intrinsic region of the diode induces a photocurrent which is sensed by a receiver circuit and converted into digital ones and zeros. The left half of Figure 4-7 is a diagram of the photodetector showing three ports: an optical port for incoming light and two electrical ports for the p and n sides of the diode. The right half of the figure is a circuit equivalent model of the photodetector, which can be translated into

Verilog-A. The photodetector is described by the following set of equations:

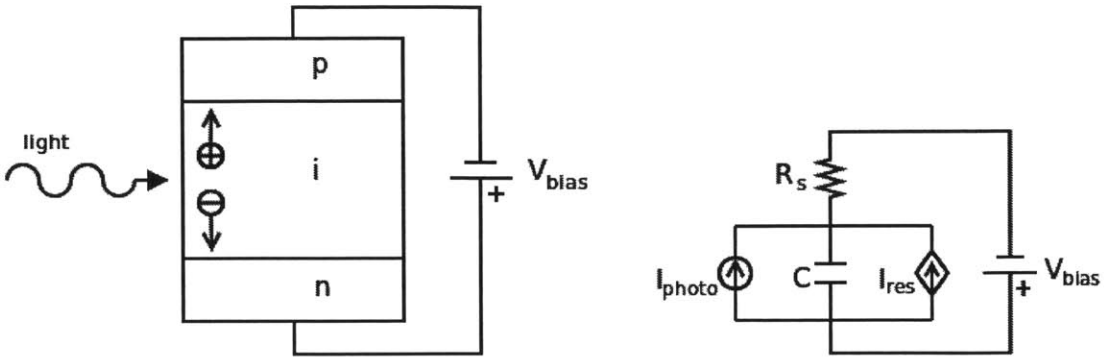

Figure 4-7: On the left is a diagram of a PIN diode showing generation of photocurrent, and on the right is the photodiode equivalent circuit.

$$
\begin{aligned}
I_{photo} &= R_{spv}|E_{in}|^2 + \frac{V_{PDbias}}{R_{dark}} \\
I_{res} &= I_s(e^{\frac{V_{PDbias}}{v_t}} - 1) \\
I_{cap} &= \frac{d}{dt}(C\,V_{PDbias}) \\
C &= \frac{\varepsilon_{Ge}A}{W_i}
\end{aligned}
$$

The first equation accounts for the photocurrent produced by incoming light. The parameter R_{spv} is the responsivity of the photodiode in Amps/Watt. R_{dark} is the equivalent resistance to account for the dark current which is assumed to be steady and noiseless for now. Finally, V_{bias} is the bias voltage on the photodiode.

The second equation is the Shockley diode equation to account for the resistive portion of the diode model. The third equation accounts for the junction capacitance in the device. However, this capacitance is computed differently from the junction capacitance of the modulator diode. The capacitance is determined by the fourth equation. This capacitor, for the first-order model, is treated as parallel plate due to the increased distance between the p and n sides because of the intrinsic region in between. A more exact model would also include the bias-voltage-dependent depletion region widths, which could add as much as 20% to the intrinsic width, as well as the parasitic capacitance to substrate.

A figure of merit of the photodetector is sensitivity: how much laser power is needed to reliably resolve each bit. One way in which the photonic link can be optimized is to find the minimal laser power needed to trigger enough current for voltage buildup to reach the receiver circuit's sense-amp latching input swing [1]. This is why it is important to continue to refine models of the photodetector and other elements.

4.6 Optical Combiner

So far, the models have been descibed as if only one wavelength is traveling through the device. However, this is not going to be the case in practical applications. In order to provide a way to simulate multiple wavelength channels simultaneously propagating through a photonic link, an optical combiner element was created.

The combiner takes inputs of light of varying wavelengths that will be present in the link, and produces an output which is the superposition of the inputs, as illustrated for two wavelengths in Figure 4-8. Although this figure includes two inputs,

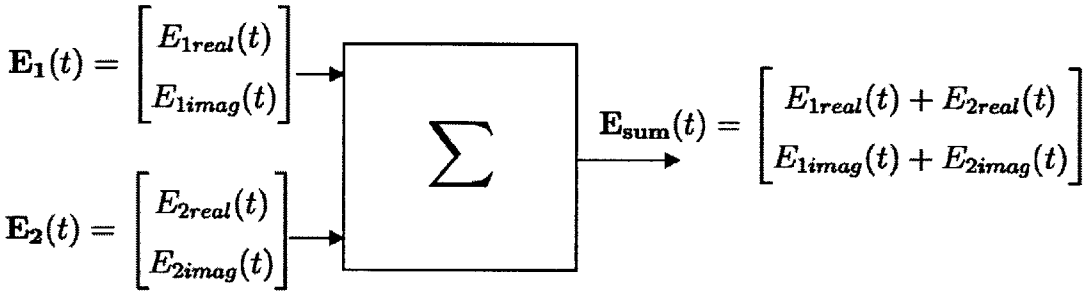

Figure 4-8: Optical combiner for superposing several wavelenths of light onto optical devices in simulation.

the combiner is actually a parametrized module where any number of inputs can be used, allowing any number of wavelengths to be combined. However, due to current limitations of Verilog-A compilation, the model needs to be recompiled each time the number of inputs is changed.

Chapter 5

Simulation Results

Once each component model was written, that component was added as an additional stage in the photonic link circuit. Simulations were run in Cadence to ensure that each model produced the correct results. Because the laser model was written first, it was tested first and used in testing the subsequent components: combiner, waveguide, modulator, and photodetector. Once proven to be functional, the components were strung together to form a complete photonic link and the link was simulated transmitting a data pattern. This chapter will showcase the simulation results for each component and for the link as a whole.

5.1 Verification of Individual Components

The following sections will describe the testbenches, device parameters, and simulations that were performed to verify functionality of each photonic component.

5.1.1 Laser

A laser producing light at the center frequency f_0 will have a real part that is constant and equal to the magnitude, and an imaginary part that is constant and zero. If a frequency offset Δf is added, then the phase difference between light of the new frequency and light of the center frequency will grow linearly in time at the rate Δf.

When this signal is represented as real and imaginary parts, they are a cosine and sine wave with period $1/\Delta f$, respectively.

To demonstrate this effect, the continuous-wave laser model was tested using the testbench shown in Figure 5-1 and it was configured with the parameters listed in Table 5.1. The output of the laser for two frequency offsets was plotted in Figure 5-2.

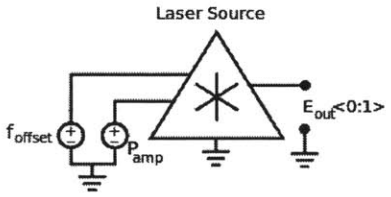

Figure 5-1: Laser testbench

Name	Value	Description
f_0	$200THz$	carrier frequency
Laser-1		
Δf_1	$8GHz$	frequency offset
λ_1	$1499.94nm$	wavelength
P_{amp1}	$100mW$	output power
Laser-2		
Δf_2	$16GHz$	frequency offset
λ_2	$1499.88nm$	wavelength
P_{amp2}	$80mW$	output power

Table 5.1: Laser parameters

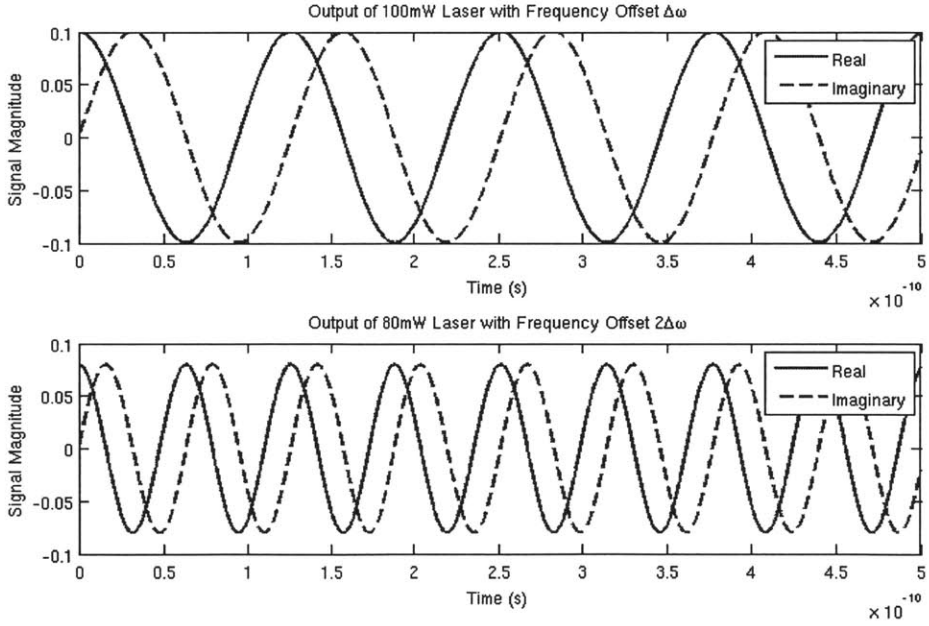

Figure 5-2: Output signals of two different laser sources.

For this simulation, the carrier center frequency was chosen to be 200THz, corresponding to a wavelength of 1500nm, a typical wavelength for photonic links. The top graph in Figure 5-2 is the output of the laser with an 8GHz offset from the center

frequency, producing 1499.94nm wavelength light. While the difference between the two wavelengths seems small, it is enough to produce a difference in transmissity of a ring filter. The bottom graph has twice the frequency offset, 16GHz, and the real and imaginary parts of the output oscillate twice as fast as in the top graph because the relative phase of the light grows twice as fast.

Larger frequency offsets will demand smaller time stepping in simulation to capture the rapid oscillations. This reduces the advantage gained from downconverting the carrier frequency to baseband, and eliminating the need to simulate 200THz oscillations of light. However, there is a limit on how large a frequency offset would need to be simulated, and it arises from the fact that all frequency channels in a link have to fit within one FSR. For a ring filter of 5μm radius, which is typical in modern processes, the FSR is 2.2THz. If the center frequency is placed in the middle of the FSR, then the frequency offset can be at most 1.1THz. This still offers a 200-fold increase in simulation time step over simulating the 200THz carrier frequency.

5.1.2 Combiner

The combiner is a theoretical device that was made to allow simulation of multiple carrier channels on the same link. This device can superpimpose an arbitrary number of carrier channels into one set of real and imaginary signals compatible for input into the modeled photonic devices. Figure 5-3 shows the testbench used for testing the combiner. Figure 5-4 plots the resulting signal when the two laser sources from Figure 5-2 are superimposed. The combined power and frequency content of the two lasers is present at the output of the combiner.

5.1.3 Waveguide

A waveguide element transmits an optical signal applying three effects: time delay, phase delay, and attenuation. The longer the waveguide is, the more pronounced these effects will be. The waveguide model was tested by comparing a laser input to the output of two waveguides of different lengths. The testbench is shown in Figure

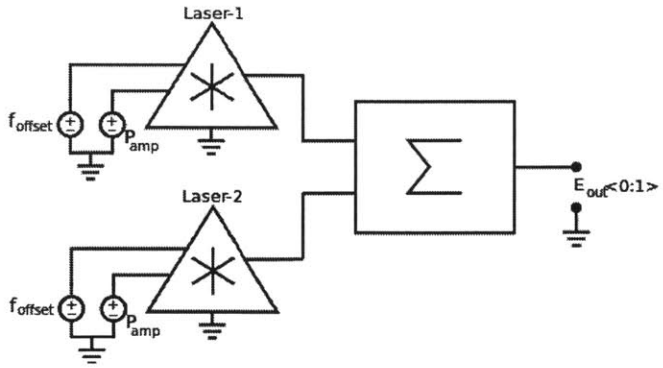

Figure 5-3: Combiner testbench

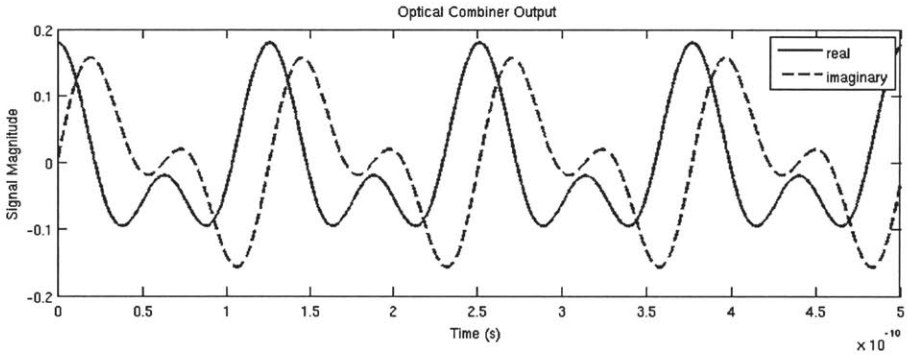

Figure 5-4: Combined output of the two lasers from Figure 5-2.

5-5. The laser input is the same as Laser-1 from Table 5.1 and the waveguide is configured as listed in Table 5.2.

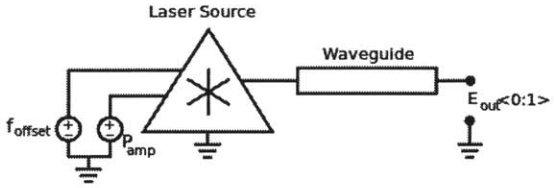

Figure 5-5: Waveguide testbench

Name	Value	Description
α	$288m^{-1}$	attenuation coefficient
n_g	4.1963	group index
L_1	$500\mu m$	waveguide-1 length
L_2	$1mm$	waveguide-2 length

Table 5.2: Waveguide parameters

This simuation was repeated on a 500μm-long and a 1mm-long waveguide, which could occur, for example, in an intra-chip link which connects circuits on one side of the die to circuits on the other side of the die. Figure 5-6 plots the output of each waveguide. The figure shows that, as expected, the effects become more pronounced with increasing length: the longer waveguide outputs a smaller amplitude and more

delayed version of the input. The real and imaginary parts of the signal experience the same effect, so to avoid crowding the graph only the imaginary part is shown.

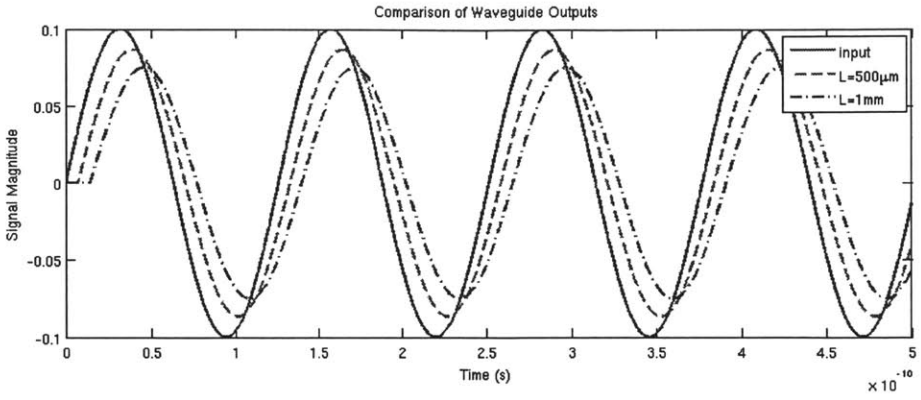

Figure 5-6: Output of two different length waveguides.

5.1.4 Modulator

The model of the modulator is able to account for two effects. The first effect is a shift in resonant frequency when voltage is applied, which allows encoding data onto the light stream. The second effect is the cyclical FSR, when the ring strikes another resonance because frequency is offset enough that the integer number of wavelengths which fit into the ring is higher by one. The testbench used to demonstrate these effects is shown in Figure 5-7, and the modulator parameter values are listed in Table 5.3.

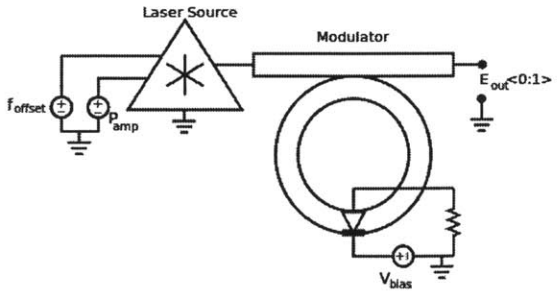

Figure 5-7: Modulator testbench

Name	Value	Description
t	0.05	coupling coefficient
L_{tot}	$30\mu m$	ring circumference
L_j	$30\mu m$	length of doped region
n_0	2.15	fitting number
n_1	$4\text{x}10^{-5}$	fitting number
α_{eff}	$60m^{-1}$	field loss coefficient
V_{bias}	$0V, 1V$	diode bias voltage

Table 5.3: Modulator parameters

Resonant Frequency Shift

For this simulation, the frequency offset of a 10mW laser source was swept from -15GHz to +15GHz while the modulator bias voltage was held constant at 0V. This was repeated for a modulator reverse-bias voltage of 1V. The output optical power is plotted in Figure 5-8.

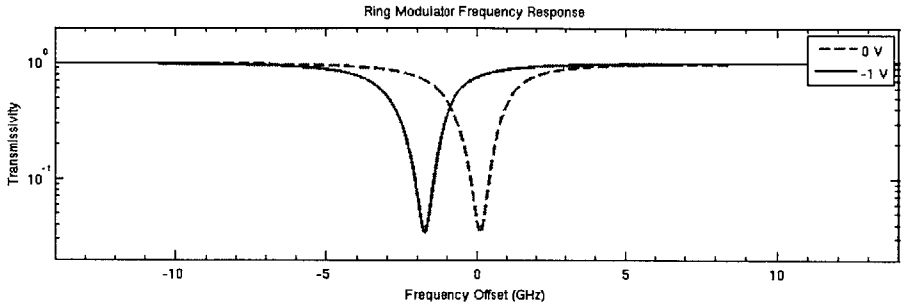

Figure 5-8: Modulator resonance shift due to applied bias.

The resonance of the ring modulator shifts by about 2GHz between the 0V and the 1V modulator bias. This provides an extinction ratio of about 12dB which is good because the models do not yet account for noise and process variations, which will degrade the performance. Models also currently do not account for nonlinear effects of power build-up within the silicon ring.

Free Spectral Range

Ring filters and ring modulators also possess a cyclical FSR which can be useful in tuning the rings, so it is important for the model to reflect this feature. This model supports the FSR by dynamically computing the effect of the device on light traveling through it instead of relying on a pre-defined transfer function. To simulate this effect, the testbench in Figure 5-7 was used again. Figure 5-9 displays the result of sweeping the frequency offset of the laser over the range 0-320GHz, without changing the bias voltage, causing the ring modulator to strike three resonances.

This sweep was performed on a ring of circumference 500μm, which is much larger than typical, but is convenient for debugging the model. The FSR of a ring is inversely

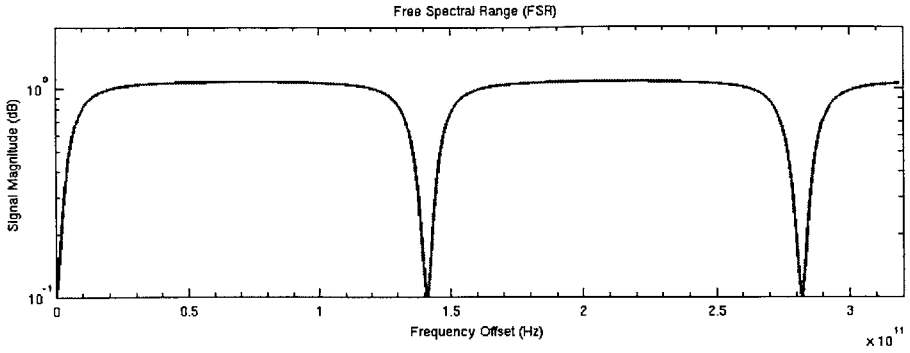

Figure 5-9: Repeating free spectral range of ring resonator.

proportional to its size, so a smaller ring has a larger FSR:

$$FSR = \frac{c}{L_{tot} n_g}$$

To show a single FSR of the 30um ring more typically used in circuits, the offset frequency would need to be swept up to 2.4THz. The 500μm ring has an FSR of 140GHz, and it took 4 minutes to run the 0-320GHz sweep for the simulation. For the 30μm ring, not only would the sweep interval be eight times wider, but smaller time steps would be required to accomodate the large frequency offset, as discussed earlier. Given that, the time to run a simulation for the 30μm ring is estimated to be on the order of 4 hours.

5.1.5 Photodetector

The photodetector is supposed to generate a photocurrent proportional to the intensity of light entering its optical input port. In the testbench shown in Figure 5-10, the laser ouput power is switched between 1mW and 10mW to stimulate the photodetector with varying intensity of light. The photodetector is configured with the parameters listed in Table 5.4.

The photodetector consists of a photodiode, so the step response of the device should have a time constant set by the junction capacitance and series resistance. To confirm this, Figure 5-11 plots the output of the photodetector when given a square

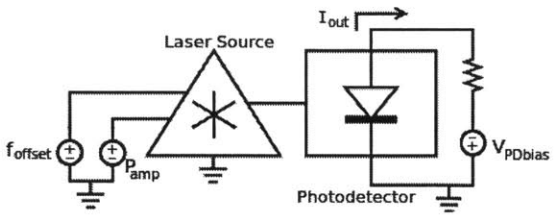

Figure 5-10: Photodetector testbench

Name	Value	Description
R_{spvty}	$1A/W$	photodiode responsivity
R_{dark}	$1M\Omega$	dark current equivalent resistance
W_i	$700nm$	intrinsic region width
L_{diode}	$10\mu m$	junction length
W_{diode}	$1\mu m$	junction width
R_{series}	$1k\Omega$	series parasitic resistance

Table 5.4: Photodetector parameters

wave input representing 20Gb/s data rate. The time constant, which can be estimated using the parameters given in Table 5.4 to be 2ps, suggests that the bandwidth of this photodetector is on the order of hundreds of gigahertz.

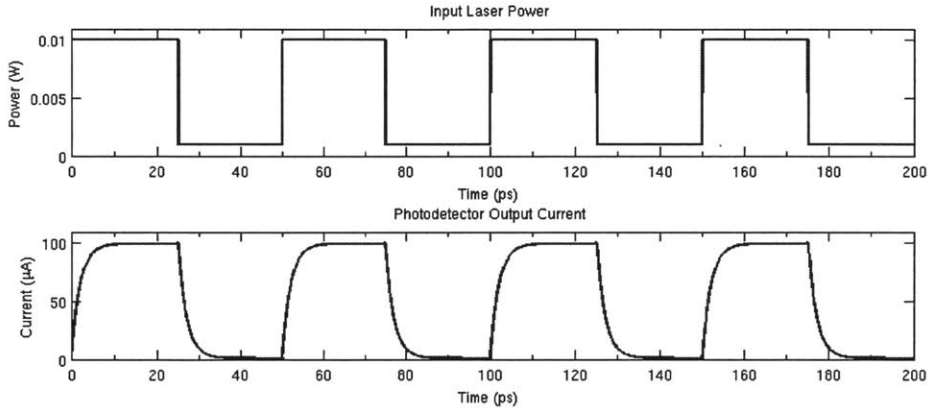

Figure 5-11: Photodetector current for varying input laser power.

5.2 Full Link Simulation

After each of the link components had a working model, the link was simulated as a whole. Figure 5-12 shows a circuit schematic of the photonic link testbench. No waveguide element is included because it would only delay and attenuate the signal, but it will not impact the shape of the signal because the model of the waveguide does not yet include any frequency-selective filtering effects. Table 5.5 summarises the device parameters used for this simulation. First, a basic test of the link's ability

to transmit data was performed. Next, a more complex data stream was transmitted to produce an eye diagram.

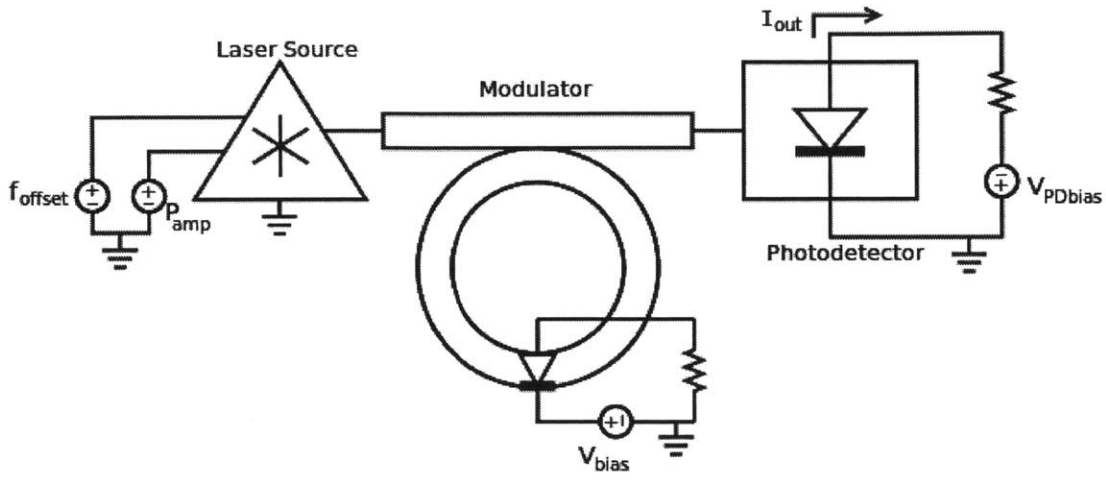

Figure 5-12: Complete photonic link testbench

5.2.1 Transient Analysis

First, a basic transient simulation was performed to see how the link would respond to on-off keying of light by the modulator. The modulator was driven by a 10GHz square wave alternating between 0V and 1V, while the laser frequency was held constant. Three signals are plotted in Figure 5-13: the voltage across the modulator diode, the optical power coming out of the modulator through port, and the current out of the photodetector.

In Figure 5-13, the output current of the photodetector closely matches the modulator output optical power which is the input to the photodetector. As discussed in Section 5.1.5, the photodetector has a fast response. Hence, the bandlimited shape of the output signal arrises from the modulator. For the modulator in this simulation, the electrical response of the diode looks much less bandlimited than the optical response, suggesting that the optical response of this modulator is the limiting factor on link data rate.

Name	Value	Description
Laser		
P_{amp}	$10mW$	optical power
f_0	$200THz$	center carrier frequency
Δf	0	frequency offset
Modulator		
t	0.05	field coupling coefficient
L_{tot}	$30\mu m$	circumference of ring
L_j	$30\mu m$	doped region length
α_{eff}	$60m^{-1}$	field loss coefficient
n_0	2.15	index fitting number
n_1	$4\text{x}10^{-5}$	index fitting number
R_s	$1k\Omega$	parasitic series resistance
Photodetector		
R_{spvty}	$1A/W$	responsivity
R_{dark}	$1M\Omega$	dark current equivalent resistance
W_i	$700nm$	intrinsic width
L_{diode}	$10\mu m$	junction length
W_{diode}	$1\mu m$	junction width
R_{series}	$1k\Omega$	parasitic series resistance
I_s	$10^{-14}A$	reverse bias saturation current

Table 5.5: Summary of device parameters

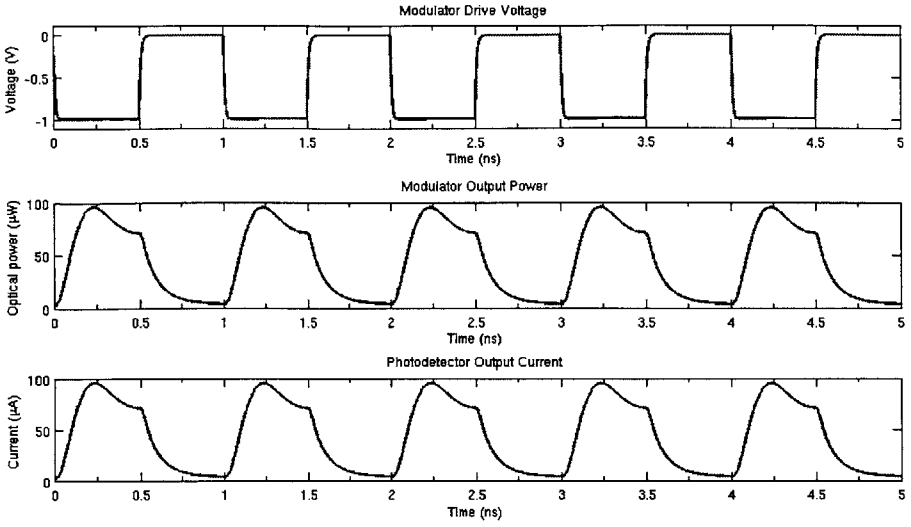

Figure 5-13: Transient simulation of the photonic link.

5.2.2 Eye Diagram

After confirming basic operation, the modulator was driven with a more complex data pattern. The data pattern, 0001011100, was designed to include every two-bit state transition to illustrate the effect of inter-symbol interference (ISI) on the link. The laser frequency was held constant while the modulator bias voltage changed between 0V and 1V with a 10GHz data rate. Figure 5-14 shows the same signals of interest as Figure 5-13. Figure 5-15 shows an eye diagram of the photodetector output current.

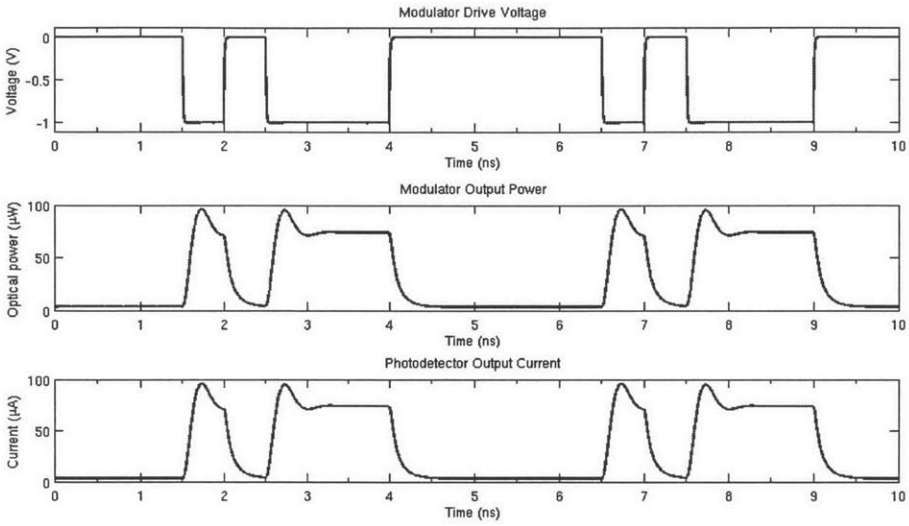

Figure 5-14: Transient simulation of the photonic link.

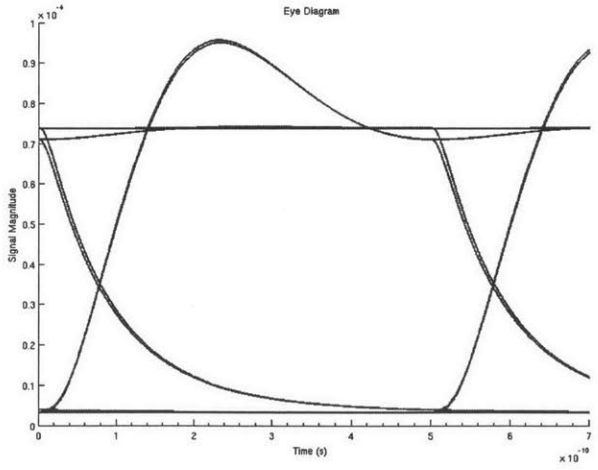

Figure 5-15: Eye diagram of photodetector output.

Chapter 6

Conclusion

Photonic links are a developing technology that promises to resolve the interconnect bottleneck of modern integrated circuits by leveraging wavelength-division multiplexing to achieve high bandwidth density and low energy per bit. Before photonic links can become a mainstream technology, models must be developed to facilitate the design of circuits and systems that use photonic devices. This thesis presented a library of first-pass Verilog-A models for components of a photonic link. The functionality of the models was demonstrated through a series of device and link simulations. These models are compatible with circuit simulators, eliminating the need for using a separate optical simulator, and allowing simulation of photonic and electronic systems side-by-side to achieve higher accuracy. These models will aid in the design and optimization of photonic link technology.

6.1 Future Work

Although a model has been created for each component of the photonic link, much work remains to be done. The second-pass models will consider more effects, such as interference and scattering at interfaces of devices, and noise and electromagnetic interference. In addition, support for thermal tuning needs to be added to allow further exploration of the tuning strategies presented in [1]. Moreover, since multiple modes of a propagating wave can be excited for a given wavelength and device ge-

ometry, support for computing the effect of higher order modes should be added like discussed in [7]. Finally, these models can be expanded to augment the CAD design flow if device layouts are added to each component in the library.

Appendix A

Verilog-A Code

A.1 Optical Discipline

```
// Optical
nature Efield
units = "E";
access = E;

`ifdef EPHASE_ABSTOL
abstol = `EPHASE_ABSTOL;
`else
abstol = 1e-6;
`endif
endnature

// Conservative discipline
discipline optical
potential Efield;
enddiscipline
```

A.2 Laser

```
module laser_cw(gnd, out, Htemp, ampin);
    inout         gnd;
    input         Htemp, ampin; // temp relative to roomtemp
    electrical    ampin;
    output  [0:1] out;
```

```
    thermal       Htemp;
    optical       gnd;
    optical [0:1] out;

    //Internal nodes
    optical [0:1] outP2C;

    // Device parameters
    parameter real gain=1e10;     // gain of temperature to frequency
    parameter real offsetfreq=0;  // offset from center frequency

    analog begin
        // magnitude
        E(outP2C[1],gnd) <+ V(ampin);
        // phase
        E(outP2C[0],gnd) <+ gain*idt(Temp(Htemp)+offsetfreq*2*`M_PI,0);
    end

    pol2cart outconv(outP2C, out, gnd);
endmodule
```

A.3 Combiner

```
module combiner(in, out, optical_gnd);
    inout optical_gnd;
    input [0:3] in;
    output [0:1] out;
    optical optical_gnd;
    optical [0:3] in;
    optical [0:1] out;

    // Internal nodes
    real outr, outi;  // Output real and imaginary parts
    genvar i;         // Index in for-loop

    analog begin
        outr = 0; // Reset running totals
        outi = 0;
        for (i=0; i<3; i=i+2) begin
            // Add ith input pair to running sums
            outr = outr + E(in[i+1],optical_gnd);
            outi = outi + E(in[i],optical_gnd);
        end
```

```
        E(out[1],optical_gnd) <+ outr;
        E(out[0],optical_gnd) <+ outi;
    end
endmodule
```

A.4 Waveguide

```
module waveguide(optgnd, inlig, outlig );
    inout  optgnd;
    input   [0:1]   inlig;
    output  [0:1]   outlig;
    optical         optgnd;
    optical [0:1]   outlig, inlig;

    // Device parameters
    parameter real L      = 0.0005;  // waveguide legnth [m]
    parameter real ng     = 4.1963;  // group index
    parameter real alphaA = 287.6;   // Field loss coefficient [m^-1]

    // Internal nodes
    optical [0:1] outNodly; // cart
    optical [0:1] ringres;
    optical [0:1] ringConv;

    pol2cart convs1(ringres, ringConv, optgnd);
    cartmul mulout1(ringConv, inlig, outNodly);

    analog begin
       //calculate the derivative term:
       E(ringres[0], optgnd) <+ 0.0;
       E(ringres[1], optgnd) <+ exp(-alphaA*L);

       E(outlig[0], optgnd) <+ absdelay(E(outNodly[0],optgnd),L*ng/`P_C);
       E(outlig[1], optgnd) <+ absdelay(E(outNodly[1],optgnd),L*ng/`P_C);
    end
endmodule
```

A.5 Coupler

```
module coupler(optgnd, inlig1, inlig2, outlig1, outlig2);
    input   [0:1]   inlig1, inlig2;
```

```
    inout           optgnd;
    output  [0:1]   outlig1, outlig2;
    optical         optgnd;
    optical [0:1]   inlig1, outlig1, inlig2, outlig2;

    // Device parameters
    parameter real t = 0.5;  // Field coupling coefficient

    // Internal nodes
    optical [0:1] Xcoup;
    optical [0:1] Xthru;
    optical [0:1] inlig1X;
    optical [0:1] inlig2X;
    optical [0:1] inlig1T;
    optical [0:1] inlig2T;
    optical [0:1] Xcoup2;

    analog begin
        E(Xcoup[0], optgnd) <+ 0.0;
        E(Xcoup[1], optgnd) <+ -t;
        E(Xcoup2[0], optgnd) <+ 0.0;
        E(Xcoup2[1], optgnd) <+ -t;
        E(Xthru[0], optgnd) <+ sqrt(1-t*t);
        E(Xthru[1], optgnd) <+ 0;
    end

    cartmul in1X(inlig1, Xcoup2, inlig1X);
    cartmul in2X(inlig2, Xcoup, inlig2X);
    cartmul in1T(inlig1, Xthru, inlig1T);
    cartmul in2T(inlig2, Xthru, inlig2T);
    cartadd comb1(inlig1T, inlig2X, outlig1);
    cartadd comb2(inlig1X, inlig2T, outlig2);
endmodule
```

A.6 Phase Shifter

```
module phase_shifter(vtop, vbot, optgnd, inlig, outlig);
    input           vtop, vbot;
    input   [0:1]   inlig;
    inout           optgnd;
    output  [0:1]   outlig;
    electrical      vtop, vbot;
    optical         optgnd;
```

```
optical [0:1]   outlig, inlig;
branch (vtop,vbot) res, cap;

// Device parameters
parameter real L        = 500e-6;  // Ring length [m]
parameter real ng       = 4.2543;  // Group index
parameter real alphaeff = 0;       // Field loss coeffcient [m^-1]
parameter real n0       = 0.0;     // Index fitting number
parameter real n1       = 0.01;    // Index fitting number
parameter real length   = 10e-6;   // Length of diode [m]
parameter real Is       = 1e-14;   // Rev-bias saturation current [A]

// Derived Parameter Declarations
real Va;
real neff;
real c, v, capacitance;
real a6, a5, a4, a3, a2, a1, a0;   // Coefficients for polynomial

// Internal nodes
optical [0:1] TshifterP;
optical [0:1] TshifterC;
optical [0:1] outNodly;

pol2cart convs1(TshifterP, TshifterC, optgnd);
cartmul  multout1(TshifterC, inlig, outNodly);

analog begin
    // initialize constants
    a6 = 0.0005e-15;
    a5 = 0.0070e-15;
    a4 = 0.0384e-15;
    a3 = 0.0921e-15;
    a2 = 0.0983e-15;
    a1 = 0.1131e-15;
    a0 = 0.3628e-15;

    // Calculate junction capacitance
    // if V(p,n) is outside the range of data then capacitance clips
    v=V(cap);
    if (v>0)
        c = a0;
    else if (v<-4)
        c = a6*pow(-4,6)+a5*pow(-4,5)+a4*pow(-4,4)+a3*pow(-4,3)+
            a2*pow(-4,2)+a1*-4+a0;
    else
```

```
            c = a6*pow(v,6)+a5*pow(v,5)+a4*pow(v,4)+a3*pow(v,3)+
                a2*pow(v,2)+a1*v+a0;
        // c is capacitance per [um] of length
        // convert length from [m] to [um] and find total capacitance
        capacitance = length*1e6*c;

        // Diode equations
        I(cap) <+ ddt(capacitance*V(cap));
        I(res) <+ Is*(limexp(V(res)/($vt))-1);

        // Calculate optical outputs
        neff = n0+n1*V(vtop,vbot);
        E(TshifterP[0], optgnd) <+ ((neff*L*2*`M_PI)*
                                    (`G_FREQ)/`P_C)%(2*`M_PI);
        E(TshifterP[1], optgnd) <+  exp(-alphaeff*L);

        E(outlig[0], optgnd)<+absdelay(E(outNodly[0],optgnd),L*ng/`P_C);
        E(outlig[1], optgnd)<+absdelay(E(outNodly[1],optgnd),L*ng/`P_C);
    end
endmodule
```

A.7 Photodetector

```
module photodetector(optgnd, vtop, vbot, inlig);
    input   [0:1]  inlig;
    inout          optgnd;
    inout          vtop, vbot;
    electrical     vtop, vbot;
    optical [0:1]  inlig;
    optical        optgnd;
    branch (vtop, vbot) res, cap, photo;

    // Device parameters
    parameter real Rspvty = 1.0;  // Photodiode responsivity
    parameter real Rdark  = 1e6;  // Dark current equiv resistance [Ohm]
    parameter real Wi  = 700e-9;  // Width of intrinsic region [m]
    parameter real len = 10e-6;   // Length of photodiode [m]
    parameter real wid = 1e-6;    // Width of photodiode [m]
    parameter real Is  = 1e-14;   // Rev-bias saturation current [A]
    parameter real Rs  = 1e3;     // Series resistance [Ohm]

    // Derived Parameter Declarations
    real Optmag;
```

```
    real eGe;                    // Dielectric constant of germanium
    real Cj;                    // Junction capacitance

    analog begin
        eGe = 16*`P_EPS0;
        Cj = eGe*len*wid/Wi;    // model as parallel plate for now

        // Diode equations
        I(cap) <+ ddt(Cj * V(cap));
        I(res) <+ Is*(limexp(V(res)/($vt))-1);

        // Calculate photocurrent
        Optmag = E(inlig[1], optgnd)*E(inlig[1], optgnd)+
                 E(inlig[0], optgnd)*E(inlig[0], optgnd);
        I(photo) <+ Rspvty*Optmag+V(photo)/Rdark;
    end
endmodule
```

Bibliography

[1] C. Sun, *Design space exploration of photonic interconnects.* M.S. thesis. Cambridge, Massachusetts: MIT, 2011. [Online]. Available: DSpace@MIT.

[2] J. Leu, *A 9GHz injection locked loop optical clock receiver in 32-nm CMOS.* M.S. thesis. Cambridge, Massachusetts: MIT, 2010. [Online]. Available: DSpace@MIT.

[3] B. Moss, *High-speed modulation of resonant CMOS photonic modulators in deep-submicron bulk-CMOS.* M.S. thesis. Cambridge, Massachusetts: MIT, 2009. [Online]. Available: DSpace@MIT.

[4] M. Georgas, *An optical data receiver for integrated photonic interconnects.* M.S. thesis. Cambridge, Massachusetts: MIT, 2009. [Online]. Available: DSpace@MIT.

[5] K. Kundert and O. Zinke, *The Designer's Guide to Verilog AMS.* Boston: Kluwer Academic Publishers, 2004.

[6] T. Smy, M. Freitas, and V. Ambalavanar, "Self-Consistent Opto-Thermal-Electronic Simulation of Micro-Rings for Photonic Macrochip Integration,"

[7] P. Gunupudi, T. Smy, J. Klein, and J. Jakubczyk, "Self-consistent simulation of opto-electronic circuits using a modified nodal analysis formulation," *IEEE Transactions on Advanced Packaging* PP(99), 1-15 (2010).

[8] T. Smy, P. Gunupudi, S. McGary, and N. Ye, "Circuit-level transient simulation of configurable ring resonators using physical models," *J. Opt. Soc. Am.* B 28, 1534-1543 (Jun 2011).

[9] T. Smy and P. Gunupudi, "Robust Simulation of Opto-electronic Systems by Alternating Complex Envelope Representations," *IEEE Transactions on TCAD* - Accepted for publication.

[10] J. Orcutt, et. al., "An Open Foundry Platform for Hight-Performance Electronic-Photonic Integration," Optical Society of America, 2012.

[11] M. Georgas, J. Orcutt, R. J. Ram, and V. Stojanovic, "A Monolithically-Integrated Optical Receiver in Standard 45-nm SOI," European Solid-State Circuits Conference, Helsinki, Finland, 4 pages, September 2011.

[12] M. Georgas, J.C. Leu, B. Moss, C. Sun, and V. Stojanovic, "Addressing Link-Level Design Tradeoffs for Integrated Photonic Interconnects," IEEE Custom Integrated Circuits Conference, 8 pages, San Jose, CA, September 2011.

[13] S. M. Sze, K. K. Ng, "Photodiodes" in *Physics of Semiconductor Devices*, 3rd ed. Hoboken, N.J. : Wiley-Interscience, 2007, ch. 13, scc. 3.